Oxidative Cross-Esterification and Related Pathways of Co-Adsorbed Oxygen and Ethanol on Pd–Au

Edward James Evans, Jr.,[†,§] Hao Li,[‡,§] Sungmin Han,[†] Graeme Henkelman,[‡] and C. Buddie Mullins*[,†]

[†]McKetta Department of Chemical Engineering and Department of Chemistry, Texas Materials Institute, Center for Electrochemistry, University of Texas at Austin, Austin, Texas 78712-0231, United States

[‡]Department of Chemistry and the Institute for Computational and Engineering Sciences, Texas Materials Institute, The University of Texas at Austin, 105 E. 24th Street, Stop A5300, Austin, Texas 78712, United States

Ⓢ *Supporting Information*

ABSTRACT: Ethanol is one of the most important industrial chemicals considering its wide range of uses. From ultrahigh vacuum (UHV) experiments, we were able to effectively produce acetaldehyde and ethyl acetate on a Pd–Au model catalyst. The presence of oxygen at the Pd–Au interface sites was found to be highly reactive for ethanol dehydrogenation, significantly increasing acetaldehyde production and promoting cross-esterification to produce ethyl acetate. Density functional theory calculations show that compared to the bare PdAu(111) surface, the presence of preadsorbed oxygen and the subsequently formed hydroxyl group leads to highly active and selective initial ethanol dehydrogenation at the O–H and α–C-H position, which was corroborated by isotope-labeling experiments. Specifically, using temperature-programmed desorption with the isotope CD_3CH_2OH, we identified C–C bond breakage through methane production. Furthermore, the simultaneous desorption of D_2 with ethyl acetate from the oxidation of CD_3CD_2OD suggests that the abstraction of hydrogen from acetaldehyde and/or ethanol is a relevant step in ethyl acetate production, which is supported by our theoretical predictions. These results shed light on the mechanistic pathways of having oxygen and ethanol coadsorbed on Pd–Au surfaces, which has significant implications for industrial applications such as fuel cells where catalytic design plays a major role in the efficiency of power production.

KEYWORDS: *Pd–Au alloy, density functional theory, dehydrogenation, esterification, temperature-programmed desorption*
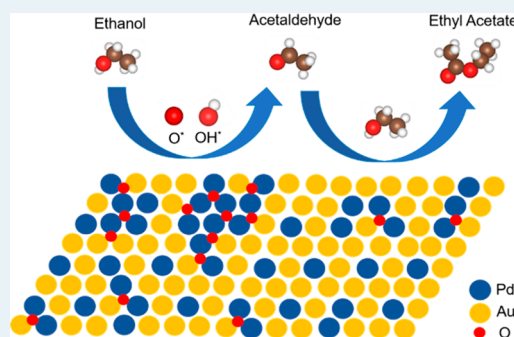
INTRODUCTION

Considering its renewability, relative ease to produce, transport, and store, its low toxicity, and its diversity of application, ethanol is a molecule of industrial significance. To contribute to the hydrogen economy, much work has been done regarding steam reforming of ethanol to produce hydrogen for fuel cells[1−3] and other uses.[3−7] Furthermore, electrocatalytic oxidation of ethanol has received much interest because of direct ethanol fuel cells.[8−10] Having use as a fuel, ethanol is also a desired product from syngas (H_2 and CO) reactions.[11−13] Many of these industrial processes require ethanol reactions in the presence of oxygen or another oxidant as part of the production or limitation of the desired products. On the industrial scale, many factors such as pressure, reactant distribution, temperature, and support material influence the efficiency, stability, product distribution, and yield of ethanol reactions. Model catalyst studies offer great control over many of these factors, enabling investigators to elucidate relevant aspects of mechanistic pathways. Given all the diversity of ethanol's use in society and the complexity of its oxidation, it is

worthwhile to investigate the oxidation of ethanol to further elucidate relevant steps in its reactions.

Esters are among the many products that can result from ethanol reactions. Esterification is a very important industrial reaction that results in the production of many common products such as biofuels, surfactants, food preservatives, cosmetics, and pharmaceuticals.[14] Biocatalysis involving enzymatic esterification has made plenty of progress in biofuel production, especially lipase-catalyzed esterification.[15] Considering the limitless access to cellulose, esterification involving this plant-based molecule has major industrial implications.[16] There is also work in biodiesel production from the esterification of oleic acid with ethanol.[17] However, some of these processes are homogeneous reactions, making it difficult to separate the catalyst from the products and reactants. Therefore, it is important to develop a better understanding of the potential mechanism of esterification of alcohols on

heterogeneous catalysts along with other potential products that affect the esterification process.

The mechanism of alcohol cross-esterification (or cross-coupling) on Au has already been investigated in model studies. Xu et al. have determined that factors such as relative alkoxide concentration and molecular size can have major effects on esterification selectivity of alcohols.[18] Additionally, density functional theory (DFT) calculations of Au have shown that ethyl acetate is a favored reaction over acetic acid production when oxidizing ethanol on an oxygen-covered Au surface.[19] Considering that palladium (i) alloys well with Au creating synergistic effects, (ii) is involved in noble metal fuel cell materials, and (iii) can effectively dissociate oxygen molecules, it is a perfect candidate to form a bimetallic material with Au for studies involving alcohol cross-esterification. Our recent combined experimental and theoretical studies have shown that as a classically well-mixed bimetallic material, Pd−Au(111) has the features of resisting carbon coking,[20] excellent C−H/O−H/C−C bond activation capacity,[20,21] and facile hydrogen desorption.[22] The alloying of Pd and Au provides both excellent bond cleavage capacity and facile hydrogen desorption because of a well-tuned surface d-band.[20] With Au's selectivity and Pd's ability to dissociate oxygen into oxygen adatoms that enables oxidation, the bimetallic Pd−Au model catalyst can be a promising material for self-esterification reactions.

In this work, we have predicted the products of ethanol (EtOH) oxidation with DFT calculations and then used ultrahigh vacuum (UHV) experiments to verify the mechanism of ethanol oxidation on our model Pd−Au surfaces. With DFT calculations, we see that esterification is preferred over acetic acid formation due to the relatively low oxygen coverage on Pd−Au ensembles. In our ethanol oxidation experiments, we see the production of similar products as seen from ethanol decomposition with a distinct production of ethyl acetate, showing esterification production from adsorbed oxygen and ethanol. Isotope labeling experiments show us that dehydrogenation is a critical step in ester evolution from the Pd−Au surface and that further decomposition of absorbed hydrocarbons can occur.

METHODS

Computational Methods. All the theoretical calculations were conducted with DFT using the Vienna Ab Initio Simulation Package. Core electrons were described by the projector augmented-wave (PAW) method.[23] The electronic exchange and correlation were described by the generalized gradient approximation (GGA) method with the Perdew−Burke−Ernzerhof (PBE) functional.[24] The Brillouin zone was described and sampled with a $3 \times 3 \times 1$ Monkhorst−Pack k-point mesh. The valence electrons were described by expanding the Kohn−Sham wave functions in a plane wave basis[25] with an energy cutoff set at 300 eV. Soft potentials were used to describe the electrons of oxygen and carbon. Geometries were considered optimized when all the forces of each atom were lower than 0.05 eV/Å. All energy barriers were calculated using the climbing image nudged elastic band (CINEB) method[26] with at least six intermediate geometries generated between the initial and final states. Convergence tests were performed on both the binding energy and CINEB calculations by reducing the force criterion and increasing the number of layers of the slab and the energy cutoff with standard PAW potentials and van der Waals corrections; no

significant changes were found for the optimized geometries or energetic trends. Details of these convergence tests can be found in our previous papers.[20,21] Spin-polarization was tested and employed for calculations of oxygen dissociation. For calculations of reaction pathways, entropic corrections were applied to the gas-phase species with a temperature of 298.15 K.

By disentangling ensemble and electronic effects as well as strain, our very recent study shows that when alloying the elements respectively with strong and weak adsorption capacities (e.g., Pd and Au), atomic ensemble effects are more significant than those of electronic (ligand) and strain.[27] Recent combined theoretical and experimental studies have also shown that for PdAu, binding energies of the most important adsorbates involved in determining the selectivity and activity for ethanol decomposition (e.g., O, H, CO, OH, EtOH, and EtOH-dehydrogenated species) are predominantly determined by the specific composition of the local surface ensemble at the binding site, while contributions from the subsurface and surface strain lead to minor changes in the adsorbate binding energy.[21,22,27−32] On the basis of these results, we do not explicitly consider the sublayer composition in our study. On the PdAu(111) alloy surfaces, the triatomic ensembles have 3-fold symmetry where Au_3, Pd_1Au_2, Pd_2Au_1, and Pd_3 are the smallest units that determine the binding site of adsorbate species.[20,33] It was found that experimental Pd−Au model catalysts, synthesized with 2 monolayers (ML) of Pd deposited on Au(111) and then heated to form a surface alloy, can be represented by a mix of predominantly $Pd_2Au_1(111)$ (Figure 1a) and some $Pd_{monolayer}(111)$ [$Pd_{ML}(111)$] (Figure
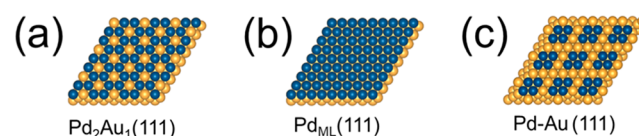
Figure 1. Modeled surfaces: (a) $Pd_2Au_1(111)$, (b) $Pd_{ML}(111)$, and (c) Pd−Au(111). Blue and gold spheres represent Pd and Au, respectively.

1b) surfaces.[20] Our previous studies, including both experiments and calculations, show that there is an adsorbate-induced driving force that stabilizes surface Pd sites on the Au(111) substrate.[34,35] Therefore, we consider these two active surfaces in our calculations to draw insight on EtOH interactions on Pd−Au interface and Pd(111)-like sites of our UHV model catalysts. To evaluate the interface effect between the triatomic ensembles of Pd_3 and Pd_2Au_1, a Pd−Au(111) surface was also modeled for oxygen dissociation and diffusion (Figure 1c). All the surfaces were modeled as slabs with (3×3) unit cells and four atomic layers. A five-layer slab model was tested in a previous study on PdAu(111) for ethanol decomposition study;[20] no significant changes were found. A vacuum layer of 12 Å was used to separate the periodic images. For each slab, the bottom two atomic layers were fixed in bulk positions, while the topmost two layers were relaxed. The lattice constants of the surface were calculated according to Vegard's law; the lattice constants of the modeled $Pd_2Au_1(111)$, $Pd_{ML}(111)$, and Pd−Au(111) were 4.05, 4.03, and 4.06 Å, respectively. Coordinates of important geometries can be found in the Supporting Information.

Experimental Methods. The molecular beam scattering ultrahigh vacuum (UHV) apparatus with a base pressure of 1 ×

10^{-10} Torr has been described in detail previously.[36,37] Briefly, the apparatus is equipped with Auger electron spectroscopy (AES) for surface elemental identification, quadrupole mass spectrometry (QMS) for detection of gaseous species, and reflection−absorption infrared spectroscopy (RAIRS) for identification of adsorbed surface species. A molecular beam source and a series of apertures are aligned to the Au(111) single-crystal sample for molecular beam impingement. The 11 mm diameter Au(111) single-crystal sample is 1.5 mm thick and is mounted to a tantalum plate that can be resistively heated to 900 K with a DC power supply regulated by a proportional−integral−differential controller. Monitoring the sample temperature with a K-type thermocouple (alumel−chromel) spot-welded to the tantalum plate, the Au(111) sample can be cooled to 77 K through thermal contact with a liquid nitrogen bath. With argon ion bombardment (2 keV) at room temperature, we removed Pd from the surface, followed by annealing to 800 K for 15 min for lattice ordering and to remove embedded argon species. Cleanliness was verified by AES with an electron beam energy of 3 keV and emission current of 1.5 mA.

To make Pd−Au model surfaces, Pd atoms were deposited onto the Au substrate at 77 K using a homemade thermal evaporator followed by annealing the surface to 500 K for 10 min under UHV conditions. The deposition rate of Pd was calibrated with a quartz crystal microbalance (QCM) controller by assuming that a thickness of one ML of Pd is equal to the diameter of a Pd atom (0.274 nm). For our experiments, the alloys of Pd and Au are denoted as Pd−Au, with the initial Pd coverage indicated as a number of monolayers. Unless otherwise noted, the Pd−Au catalyst will have 2 ML of Pd for its initial coverage.

On our 2 ML Pd−Au surface, we previously showed that the active surface contains 74.9% Pd−Au interface sites and 25.1% Pd(111)-like sites using H_2 temperature-programmed desorption (TPD).[20,22] The epitaxial layer-by-layer mechanism suggests that alloy formation is not prevalent until annealing at which point the Pd atoms diffuse into the Au(111) subsurface.[38]

In this study, both oxygen and EtOH were impinged onto our surface held at 77 K via molecular beam using the same nozzle for both molecules for consistency. To produce the TPD spectra, we heated the Pd−Au sample at 1 K/s while monitoring the products and reactants with the QMS. The following products and unreacted reactants were monitored using the following QMS signals: EtOH (m/z = 31 and 45), acetaldehyde (m/z = 29, 44, and 15), ethyl acetate (m/z = 43), CO (m/z = 28), H_2 (m/z = 2), CO_2 (m/z = 44), and methane (m/z = 15, 16). To ensure determination of the proper product, QMS signals for other potential products were also investigated throughout the TPD experiments: formaldehyde (m/z = 29, 30), formic acid (m/z = 29, 46), ethane (m/z = 27, 28), ethylene (m/z = 26, 27, 28), acetic acid (m/z = 43, 60), ethylene oxide (m/z = 29, 44, 15), methyl formate (m/z = 60), ethyl formate (m/z = 27, 28, 29), ketene (m/z = 14, 42), and methyl acetate (m/z = 43, 74).

■ RESULTS AND DISCUSSION

Theoretical Results. To evaluate oxygen activation on the catalytic surface, CINEB calculations were performed to calculate the oxygen dissociation and diffusion pathways on the three PdAu(111) surfaces as illustrated in Figure 1. It can be clearly seen from Figure 2 that oxygen dissociation on
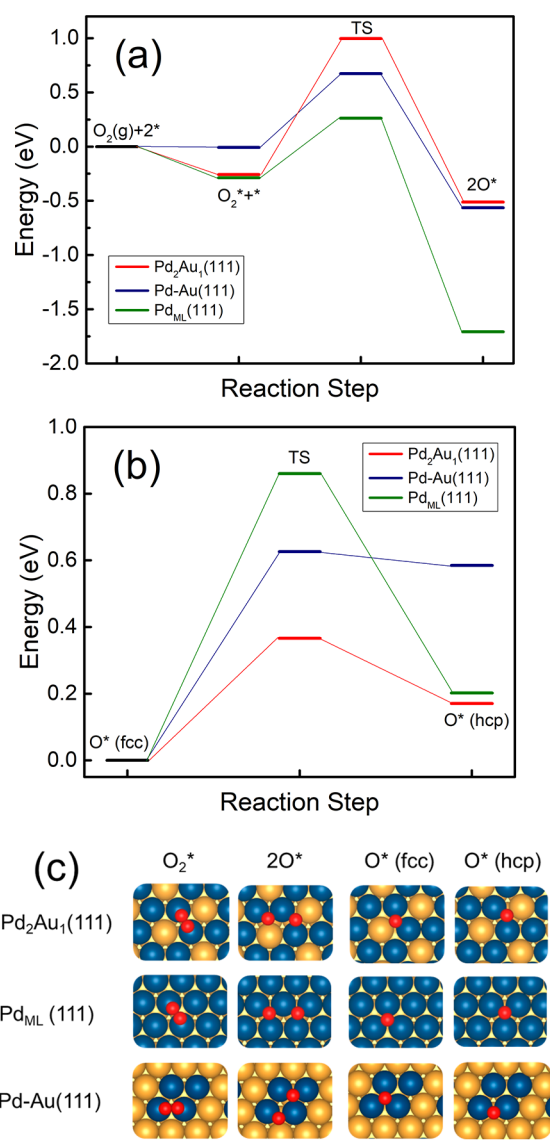
Figure 2. (a) Oxygen dissociation pathways on $Pd_2Au_1(111)$, Pd−Au(111), and $Pd_{ML}(111)$. (b) Adsorbed oxygen diffusion from an fcc site to the adjacent hcp site on the three PdAu(111) surfaces. The oxygen diffuses on Pd−Au(111) was modeled from a triatomic ensemble of Pd_3 to Pd_2Au_1. (c) Initial and final states of all the reactions shown in (a,b). Blue, gold, and red represent Pd, Au, and O, respectively.

$Pd_2Au_1(111)$ is rather difficult with an energy barrier ∼1.25 eV. This is similar to our previous conclusion that small Pd−Au surface ensembles do not readily activate oxygen.[30] In contrast, on Pd−Au(111) and $Pd_{ML}(111)$, the activation barriers are much smaller (∼0.68 and 0.55 eV, respectively). These results indicate that oxygen is more readily activated at the Pd(111)-like sites and the boundary sites between Pd and Au ensembles. Meanwhile, the oxygen diffusion energy barriers calculated on the three surfaces show that O* has a relatively high barrier to diffuse from the Pd_3 site to the Pd_2Au_1 interface site, but it is easier to diffuse between two Pd_2Au_1 ensembles (Figure 2b). Therefore, we deduce that O* at the Pd−Au interface site on our experimental model catalysts most likely originates from the O_2 dissociation at the boundary between Pd and Au ensembles, as in the pathway on Pd−Au(111) (Figure 2c). Considering that EtOH and EtOH-dehydro-
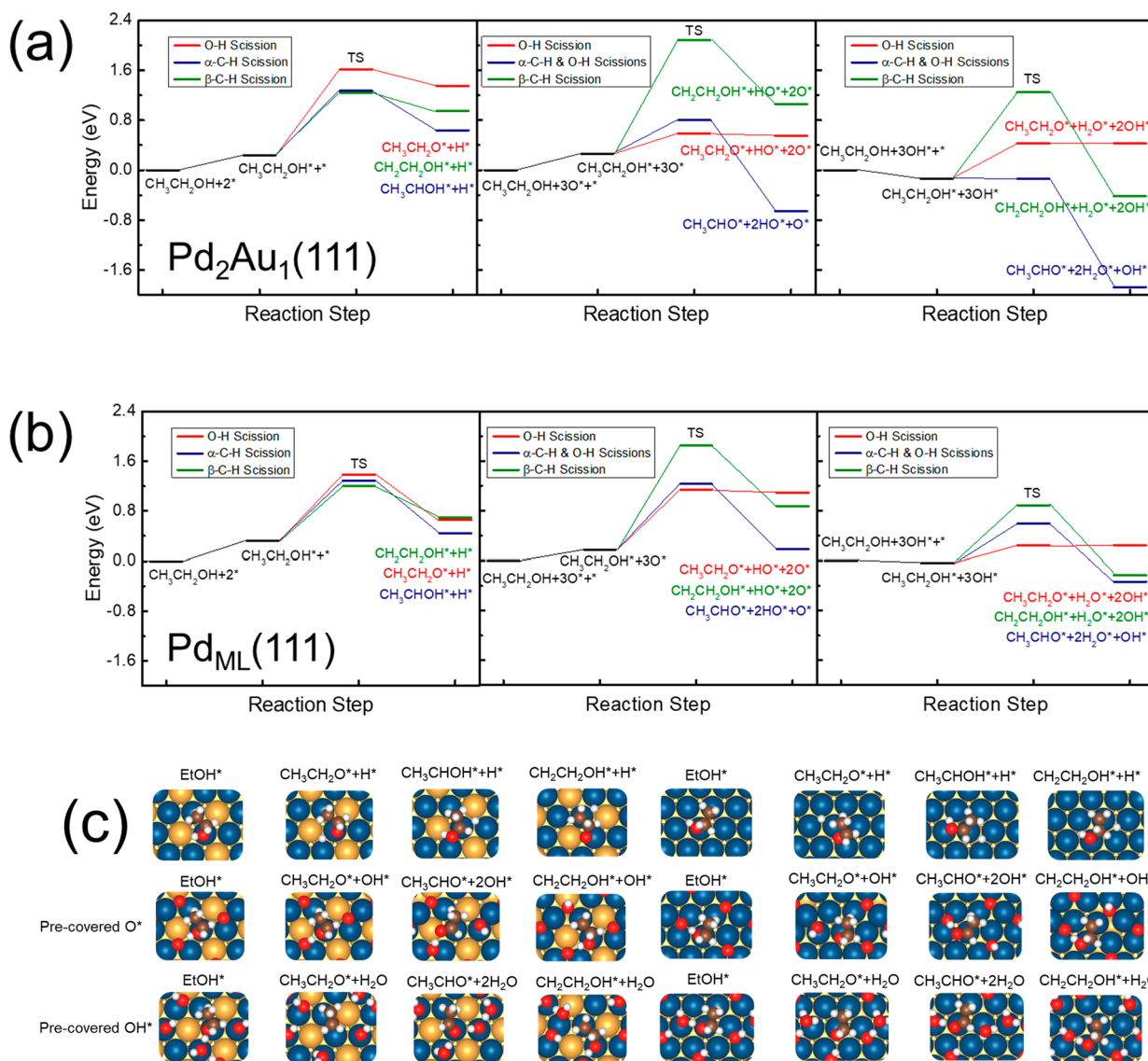
Figure 3. Ethanol initial dehydrogenation on (a) Pd$_2$Au$_1$(111) and (b) Pd$_{ML}$(111). The left, middle, and right frames, respectively, represent the reactions on bare, 1/3 oxygen precovered, and 1/3 hydroxyl precovered surfaces. (c) Initial and final states of all the reactions shown in (a,b). Blue, gold, brown, red, and white spheres represent Pd, Au, C, O, and H, respectively.

genated species have relatively weaker binding energies on PdAu surfaces,[20] our theoretical results suggest that the Pd(111)-like sites should have relatively high oxygen coverage while Pd−Au interface sites have less due to the lower oxygen affinity of Au. These calculations are beneficial in providing insight as to the sites in which oxygen adatoms are present and the local environment of EtOH dehydrogenation on our experimental surface.

The first step for EtOH oxidation is the initial dehydrogenation of EtOH. Both the activity and selectivity of this step could significantly determine the predominant product for EtOH oxidation. Our previous studies have found that on Pd−Au(111) surfaces, the initial dehydrogenation barrier generally decreases with increase of the Pd ensemble size.[21,39,40] Meanwhile, different geometries of the PdAu ensemble could lead to different initial dehydrogenation selectivities.[21,22] However, very few previous studies have discussed the activity and selectivity of EtOH dehydrogenation with preadsorbed oxygen and the (subsequently formed) hydroxyl.[19,41] Here, we calculated the reaction pathways for EtOH initial dehydrogen-

ation on the bare, oxygen precovered, and hydroxyl precovered surfaces. Since the modeled Pd$_2$Au$_1$(111) and Pd$_{ML}$(111) include the same surface ensembles as Pd−Au(111), we only evaluate the dehydrogenation reactions on Pd$_2$Au$_1$(111) and Pd$_{ML}$(111). Figure 3 shows the initial dehydrogenation pathways of EtOH at O−H, α-C−H, and β-C−H. To the best of our knowledge, there are a number of interesting and notable dehydrogenation features that have not been widely discussed in the literature:

(i) Both precovered oxygen and hydroxyl significantly lower the energy barrier of O−H and α-C−H scissions, while significantly increasing the energy barrier of β−C-H scission. Noting that the initial dehydrogenation at the β-C−H position has previously been found to be a favorable, but also unwanted, step on many metallic surfaces,[21,40] the promoter effect provided by O* and OH* can tune this selectivity back to O−H and α-C−H bond scission, which is supported by the deuterated EtOH experiments to be discussed later in the paper.

Because the optimized EtOH adsorption geometries are still highly similar among these three types of surfaces (Figure 3c), it can be concluded that these changes on the selectivity do not originate from the difference on the adsorption geometry.

(ii) Although it was widely believed that higher percentages of a strongly adsorbing element (e.g., Pd) on the surface could lead to higher decomposition activity of the adsorbate on the bare surface (Figure 3a,b, left frames),[20−22] the promoter effect by O* and OH* could increase the activity at the Pd−Au interface as compared to Pd(111)-like sites (Figure 3a,b, middle and right frames) for EtOH oxidation.

(iii) Though the adsorption energies of EtOH are negative on all the surfaces, the adsorption free energy of EtOH (after being applied with gas-phase entropic corrections) on both $Pd_2Au_1(111)$ and $Pd_{ML}(111)$ are endothermic (Figure 3a,b, left and middle frames). However, because of the hydrogen bonding effect of the formed OH*, the adsorption of EtOH to the surface covered by OH* becomes exothermic (Figure 3a,b, right frames), suggesting EtOH consumption at lower temperatures and more facile final product formation.

(iv) With two present oxygen/hydroxyls near the EtOH on $Pd_2Au_1(111)$ and $Pd_{ML}(111)$, there is an unusual but favorable initial dehydrogenation step that directly forms acetaldehyde by activating O−H and α-C−H in one elementary step, which is also a favorable step previously found by Liu et al. on Pt(111).[42] This shows that the formation of acetaldehyde should be facile and observable in TPD experiments.

The EtOH initial dehydrogenation features shown above indicate that $Pd_2Au_1(111)$ is highly active and selective for EtOH partial oxidation, leading to the formation of alkoxide or acetaldehyde. Our follow-up calculations also show that the continuous dehydrogenation of alkoxide with precovered oxygen on $Pd_2Au_1(111)$ also preferably forms acetaldehyde with a barrier of ∼0.01 eV (Figure S1). These pathways to facile acetaldehyde production are corroborated experimentally as discussed later. With the previous combined theoretical and experimental conclusion that the bare Pd−Au surface could also lead to C−C bond cleavage of the highly dehydrogenated CHCO* at a temperature lower than 300 K,[20] it is expected that the continuous dehydrogenation of acetaldehyde could lead to the formation of CH₃CO*, which is a key reactant for forming ethyl acetate through a cross-coupling mechanism with alkoxide. Due to the high computational cost and the combinatorial complexity of the potential energy surfaces, we did not include the calculations of subsequent dehydrogenations in this study.

To evaluate the formation of ethyl acetate, CINEB calculations were used to find the reaction pathway of the cross-coupling reaction between CH₃CO* and CH₃CH₂O*, as indicated by the previous study of Friend et al. on Au(111).[18] Our results show that cross-coupling requires a relatively low activation energy on both $Pd_2Au_1(111)$ (0.21 eV) and $Pd_{ML}(111)$ (0.16 eV), while in the presence of precovered oxygen, the activation barriers were further decreased to near-zero (Figure 4). We also evaluated the formation of acetic acid, as shown in Figure S2. As expected, the formation of acetic acid is also facile with the presence of an oxygen or hydroxyl nearby. However, because the oxygen and hydroxyl will be
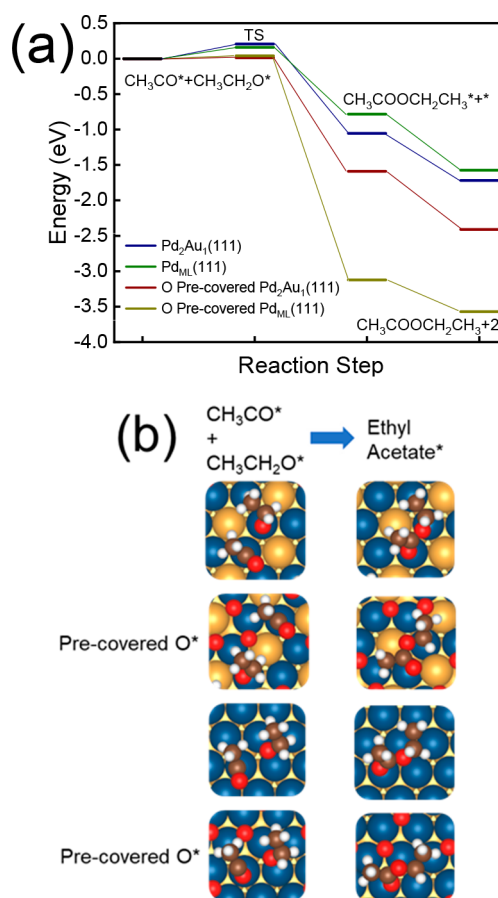
Figure 4. Reaction pathways of ethyl acetate formation through a cross-coupling mechanisms on $Pd_2Au_1(111)$ and $Pd_{ML}(111)$. Both bare and 1/3 oxygen precovered surfaces are considered for the calculations. (b) Initial and final states of all the reactions shown in (a). Blue, gold, brown, red, and white spheres represent Pd, Au, C, O, and H, respectively.

consumed after multiple dehydrogenation steps and the oxygen/hydroxyl coverage is lower on PdAu(111) than previous studies on Pd(111), which is due to a weaker O binding,[27] we expect that the formation of acetic acid is more difficult than ethyl acetate. This is in agreement with the conclusion from a previous study by Friend et al., that low oxygen coverage on Au would lead to ester formation while higher oxygen coverage would increase the formation of acetic acid and reduce the formation of ester.[43] Our CINEB calculations also show that acetic acid tends to desorb rather than decompose (Figure S3) but would be observable if it was formed in our experiments, as shown in acetic acid TPD experiments in Figure S4. Without the competing pathway of acetic acid formation, cross-coupling reactions between CH₃CO* and CH₃CH₂O* could be facile, independent of the surface alloy composition. Since the cross-coupling reaction requires more than two adsorption sites (Figure 4b), it is expected that higher oxygen coverage would hinder this reaction due to the higher oxygen diffusion barrier and the more facile formation of acetic acid.

We also evaluated other possible cross-coupling pathways such as CH₃CHO* + CH₃CH₂O*(Figure S5), with the assumption that ethyl acetate could be formed through the dehydrogenation of the hemiacetal-like intermediate, which has been a notable proposed coupling mechanism of alcohols

with aldehydes.[44] Our results show that these couplings are facile as well with coupling barriers similar to those in Figure 4a. Given that these pathways have similar and low-energy barriers for coupling, we suspect multiple pathways are possible once the oxygen and hydroxyl around the dehydrogenated EtOH species is mostly consumed. Therefore, since the cross-coupling between CH_3CO^* and $CH_3CH_2O^*$ is energetically facile and is the most straightforward way to form ethyl acetate, we mainly discuss this pathway in this paper, but we do not delegitimize other routes. It also should be noted that there are other well-known mechanisms that form esters such as the Tishchenko reaction[45] using a solution-phase homogeneous catalytic process. However, given that a surface cross-coupling mechanism proposed by Friend et al. has the gas-phase heterogeneous catalytic mechanism is more similar to our system,[43] we only evaluate the cross-coupling pathway in our theoretical study.

Experimental Results. Oxidative dehydrogenation of alcohols is an industrially relevant reaction that has been seen under various conditions.[46−48] Noble metals such as Ru,[49−51] Pt,[52,53] Pd,[53−58] and Au[54−56,59−62] have garnered much attention because of their high activity and selectivity. For ethanol, oxidative dehydrogenation has been crucial for the formation of products such as acetaldehyde, acetic acid, and ethyl acetate, especially for Cu that is relatively inexpensive, environmentally friendly, and has respectable activity.[63−67] In this work, we have used a Pd−Au catalyst to produce acetaldehyde and ethyl acetate through oxidative dehydrogenation of ethanol.

The theoretical insights described above indicate that the formation of acetaldehyde and ethyl acetate is facile on oxygen/hydroxyl precovered Pd−Au(111) surface, especially at Pd_2Au_1 interface sites. To experimentally investigate EtOH oxidative cross-coupling on our Pd−Au surface, we exposed EtOH to the surface at 77 K with and without previously exposing the surface to O_2, as shown in Figure 5. Oxygen was adsorbed until saturation on the surface at 77 K using a modified King and Wells experiment prior to EtOH exposure, as shown in Figure S6. There is clear EtOH consumption as the area under the peak associated with the EtOH feature decreases by 50% with coadsorbed oxygen as compared to without oxygen. Additionally, a second EtOH feature arises at about 160 K as seen in previous work,[22] and the primary EtOH feature decreased by 5 to 200 K. We attribute both of these phenomena to the presence of oxygen adatoms and reacted products decreasing EtOH's interaction with the Pd−Au surface enabling desorption at a lower temperature.

The two most notable EtOH products observed in this study are acetaldehyde ($m/z = 29$) at 185 K and ethyl acetate ($m/z = 43$) at 240 K, as shown in Figure 5a. EtOH has a $m/z = 29$ mass fragment also, which contributes to the majority of the $m/z = 29$ feature with only EtOH on the Pd−Au surface. Acetaldehyde has also been seen as a dehydrogenation product on Pd−Au model catalysts,[22] so there may be a small contribution of acetaldehyde production in the absence of O_2 on the surface. However, there is a notable increase in acetaldehyde production on the oxygen precovered surface, adding validity to our assertion that oxygen and hydroxyl groups aid in EtOH dehydrogenation based on the DFT calculations shown in Figure 3. On a surface precovered with oxygen, Pd(111) does produce acetaldehyde[68] despite the fact that no aldehyde species are formed in the absence of oxygen on this surface.[69] However, on Pd(110) with O_2, there was no
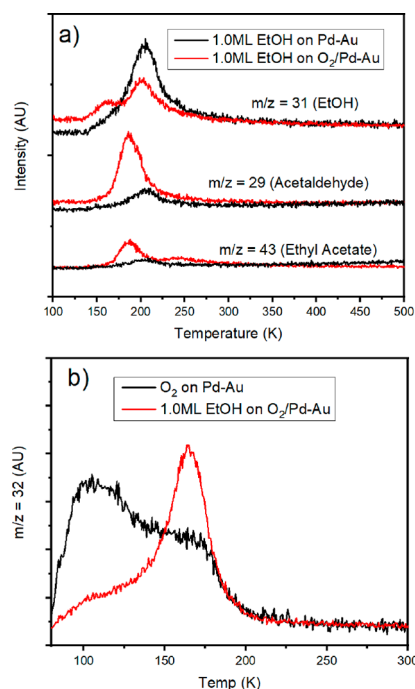
Figure 5. (a) Acetaldehyde ($m/z = 29$) and ethyl acetate ($m/z = 43$) production after 1.0 ML of EtOH ($m/z = 31$) exposure on oxygen-covered Pd−Au. (b) Oxygen ($m/z = 32$) TPD with and without EtOH on Pd−Au surface.

production of acetaldehyde despite the fact that there was surface acetate observed.[70] This surface acetate was said to further decompose into CO_2, H_2, and surface carbon instead of forming acetaldehyde or acetic acid. Furthermore, we were not able to observe any acetate species by its characteristic feature at about 1520 cm^{-1} in any of our reflection−absorption infrared spectroscopy experiments (Figure S7).

The production of ethyl acetate ($m/z = 43$) at 240 K was confirmed by impinging ethyl acetate on the Pd−Au surface and monitoring its desorption (Figure S8). Acetaldehyde contributes to the mass fragment at $m/z = 43$, which is responsible for the 185 K peak for this mass. The fact that it desorbs at the same temperature (240 K) as resulting from oxygen and ethanol coadsorption shows that the TPD feature due to oxidative cross-coupling is desorption-limited. The Friend group has previously reported oxidative cross-coupling of small alcohols on Au(111) catalysts,[18,43] but esterification was not observed on Pd-based model catalysts.[68,70,71] This leads us to believe that Au has a critical role in the mechanism of cross-coupling.

One notable observation is that we do not readily see acetic acid from ethanol oxidation at temperatures up to 700 K. Liu et al. observed acetic acid at 550 K during TPD after dosing EtOH on O/Au(111),[43] although it was not seen by Gong et al.[72] Additionally, Davis et al. produced acetic acid on their oxygen-covered Pd(111) surface, showing desorption at 280 and 410 K.[68] Despite the fact that Pd induces O_2 adsorption and dissociation, it is not completely determining the mechanistic pathway of ethanol oxidation as Au is playing a significant role in the selectivity. With our theoretical work showing that acetic acid production is facile with a nearby oxygen or hydroxyl, the fact that we do not see acetic acid production provides insight into the makeup of our surface. As stated previously, we suggest that acetic acid is more likely to

be produced when oxygen is in excess. In this work, we did not produce acetic acid at any EtOH coverage on our oxygen-saturated surface, suggesting that our oxygen coverage may be lower than in previous work on other surfaces. Another potential reason for the difference in acetic acid production is the different methods of putting oxygen on the catalytic surface. To activate Au(111) surfaces, atomic oxygen was deposited on the surface through the use of an RF generator or ozone. On the Pd(111) surface, oxygen was backfilled onto the surface at room temperature as opposed to exposed via a molecular beam at 77 K. In both cases, the oxygen dissociates on the surface to become oxygen adatoms. Furthermore, the consumption of oxygen and hydroxyl groups by the dehydrogenation of EtOH reduces the availability of oxygen to be used for acetic acid production. Regardless, despite the production of acetic acid on both Au(111) and Pd(111), we are not able to see its production on our Pd–Au surface, leading to more selective esterification.

When conducting oxidative cross-coupling, we noticed a difference in the oxygen desorption when EtOH was exposed to the Pd–Au surface, displayed in Figure 5b. Han observed two O_2 features in his study on O_2 activation on Pd–Au surfaces.[73] He attributed the 105 and 165 K features to desorption from the Pd–Au interface sites and from the Pd(111)-like island sites, respectively. This is in qualitative agreement with the theoretical results that Pd(111)-like sites have higher oxygen association and diffusion barriers than the Pd–Au interface sites (Figure 2). However, in our oxygen TPD on the 2 ML Pd–Au surface, there is more oxygen desorption from the Pd–Au interface sites. Guided by our DFT calculations to describe the Pd–Au surface, we attribute this to a larger percentage of Pd–Au interface sites on our catalytic surface. Although there could be other contributing factors that lead to this phenomenon, we believe that much of our surface has small Pd ensembles with some Pd(111)-like sites that can adsorb and dissociate oxygen, but there are significantly more Pd–Au interface sites on the surface that are involved in this process. When impinging EtOH on the oxygen-covered surface, the O species from the Pd–Au interface sites appear to be selectively consumed with the addition of EtOH as the Pd–Au interface site oxygen feature decreases. This is consistent with the DFT calculations in Figure 3, showing that the oxygen and hydroxyl groups are more active at the Pd–Au interface sites.

To investigate the phenomenon of oxidative cross-coupling further, we put EtOH and acetaldehyde on the Pd–Au surface to see if ethyl acetate would form, as shown in Figure 6. With the coadsorption of EtOH and acetaldehyde, there is a broad feature starting at 225 K and ending at 350 K, but the production is lower than that from EtOH oxidative cross-coupling. Also, these features could be due to the acetaldehyde polymerization,[74,75] so the process of esterification may not be occurring at all. This highlights the significance of the ability of oxygen and hydroxyl groups to readily dehydrogenate EtOH to produce alkoxide and acetyl intermediates, which are needed to produce ethyl acetate. As shown in Figure 5a, EtOH on Pd–Au in the absence of oxygen does not produce nearly as much acetaldehyde. Additionally, our DFT calculations (Figure 3) emphasize the enhancement of dehydrogenation of EtOH with oxygen and hydroxyl species on the surface. This highlights the important role an oxidant can play in the cross-esterification process and the selectivity of ethanol oxidation.
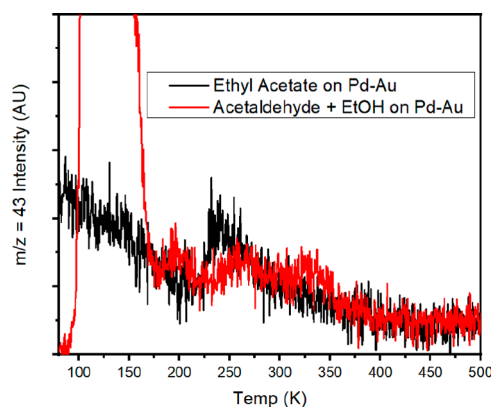

Figure 6. Ethyl acetate desorption compared to production by EtOH and acetaldehyde cross-coupling on Pd–Au.

Additionally, we observed the production of water (m/z = 18), methane (m/z = 16), carbon monoxide (m/z = 28), hydrogen (m/z = 2), and carbon dioxide (m/z = 44), which are shown in Figure S9. Previously, we have seen the production of methane, CO, and hydrogen from EtOH decomposition,[22] so we suspect some contribution of the signal to these masses from this reaction. The formation of CO_2 does show that some complete oxidation is possible on our surfaces. Water is produced from the dehydrogenation from oxygen and hydroxyl groups. The water that is shown in the absence of oxygen is due to the water from the background adsorbing on the surface prior to heating the sample. Isotope-labeling experiments provide more insight into this reaction.

To obtain more mechanistic insight, we used the EtOH isotopes CD_3CH_2OH and CD_3CD_2OD as shown in Figure 7a,b, respectively. In Figure 7a, relevant masses for methane and water are plotted during the oxidation of EtOH and CD_3CH_2OH. For EtOH, we see the production of methane (m/z = 16) peaking at 315 K. Additionally, we see the production of H_2O (m/z = 18) desorbing at 165 K. This is the same temperature where we observed O_2 desorption. Considering that the water production is a result of dehydrogenation from the oxygen and hydroxyl groups, it stands to reason that these molecules may be observed at the same time. For CD_3CH_2OH, we see the production of CD_3H (m/z = 19). This reinforces the fact that the C–C bond can break which was shown in our previous work, but also that the active methyl groups can scavenge hydrogen adatoms on the surface to produce methane. With the decreasing signal from methane fragments, this supports the production of methane. Additionally, we see the production of H_2O, but there is no D_2O formed. This indicates that dehydrogenation from oxygen species is more prominent on the hydroxyl hydrogen and α-carbon, which was shown from our calculations in Figure 3. It is worth noting that the signal for m/z = 17 and 20 were not investigated for EtOH because of the fact that no relevant product or reactant is expected to appear at those masses.

In Figure 7b, we show the TPD spectra of products from the oxidation of CD_3CD_2OD on the oxygen-covered Pd–Au surface at 77 K. We see the production of D_2O (m/z = 20) that was not present when oxidizing CD_3CH_2OH, supporting the affinity toward dehydrogenation from the hydroxyl group and the α-carbon, in agreement with our DFT calculations (Figure 3). More importantly, the production from HD (m/z = 3) and D_2 (m/z = 4) may provide insight into the mechanism of ethyl acetate production. We see two major features for HD
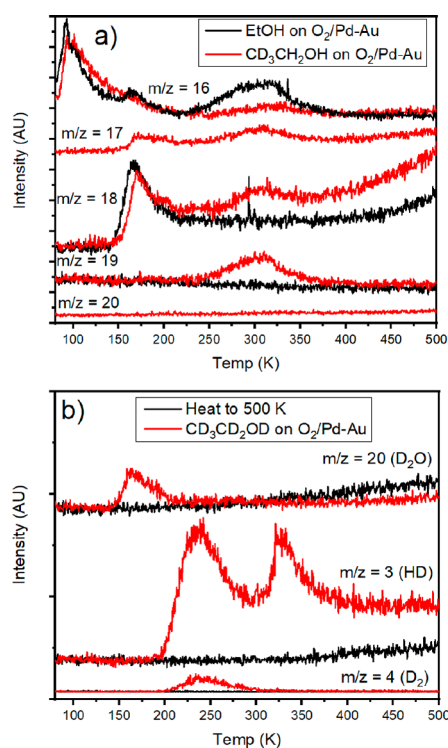
Figure 7. (a) TPD spectra of masses relevant to water and methane production from the oxidation EtOH and CD_3CH_2OH on Pd−Au. (b) TPD spectra of D_2O, HD, and D_2 from the oxidation of CD_3CD_2OD on Pd−Au.

production. The high-temperature HD feature comes off the surface at approximately 330 K. Considering that it appears after methane desorption at 310 K, we believe this feature is due to C−H bond breaking of the methyl group that resulted from C−C bond breakage. Additionally, HD and D_2 at 235 K desorb at a similar temperature as ethyl acetate. When cross-coupling occurs, dehydrogenation occurs from acetaldehyde and can occur from ethanol unless the alkoxide is the intermediate in the esterification process. The presence of D_2 suggests that the dehydrogenation from ethanol and acetaldehyde is prevalent enough that adsorbed deuterium atoms can recombine instead of being scavenged by H adatoms. Considering that H and D mobility is fairly facile at this temperature and ethanol is dehydrogenated to acetaldehyde at lower temperatures on this surface, we believe this D_2 production may suggest the onset of acetaldehyde dehydrogenation that results in ethyl acetate. Furthermore, this coincides with our theoretical calculations in which we found that ethyl acetate formation has a significantly lower energy barrier than EtOH dehydrogenation (Figures 3 and 4).

CONCLUSIONS

In this study, we have provided insight into potential pathways of coadsorbed oxygen and ethanol and cross-esterification on a Pd−Au model catalyst, using combined theoretical and experimental methods. Our DFT calculations show that with precovered oxygen and hydroxyl, the Pd−Au surface is active for EtOH dehydrogenation and acetaldehyde production. Additionally, the coexistence of the alkoxide and the acetyl intermediate makes ethyl acetate production a facile process. Our UHV experiments in which oxygen and ethanol are coadsorbed on the Pd−Au surface show a significant increase

in acetaldehyde production, which promotes the production of ethyl acetate. Our isotope experiments showed the production of water and methane and highlighted the onset of acetaldehyde dehydrogenation, leading to the production of ethyl acetate. We hope that this study provides insight into the diversity of factors at play in ethanol's oxidative mechanism while showcasing the nuances involved in adjusting its selectivity and invoke creativity in effective catalytic design to maximize production of their desired products.

ASSOCIATED CONTENT

Supporting Information

The Supporting Information is available free of charge on the ACS Publications website at DOI: 10.1021/acscatal.8b04820.

> Additional information regarding the dehydrogenation of CH_3CHO*; formation and dehydrogenation of acetic acid; TPD of acetic acid at various coverages on Pd−Au; cross-coupling pathways to form a hemiacetal-like intermediate; modified King and Wells experiment with O_2; RAIRS of EtOH with and without oxygen on Pd−Au; comparison of ethyl acetate desorption with its production from O_2 and EtOH coadsorbed on the Pd−Au surface; TPD of the H_2, CO, CO_2, and CH_4 from EtOH with and without oxygen on the surface; coordinates for the geometries used for theoretical calculations (PDF)

AUTHOR INFORMATION

Corresponding Author
*E-mail: mullins@che.utexas.edu.
ORCID
Graeme Henkelman: 0000-0002-0336-7153
C. Buddie Mullins: 0000-0003-1030-4801
Author Contributions
§(E.J.E., H.L.) These authors contributed equally.
Notes
The authors declare no competing financial interest.

REFERENCES

(1) Vaidya, P. D.; Rodrigues, A. E. Insight into Steam Reforming of Ethanol to Produce Hydrogen for Fuel Cells. *Chem. Eng. J.* **2006**, *117*, 39−49.
(2) Frusteri, F.; Freni, S. Bio-Ethanol, a Suitable Fuel to Produce Hydrogen for a Molten Carbonate Fuel Cell. *J. Power Sources* **2007**, *173*, 200−209.
(3) Nanda, S.; Rana, R.; Zheng, Y.; Kozinski, J. A.; Dalai, A. K. Insights on Pathways for Hydrogen Generation from Ethanol. *Sustain. Energy Fuels* **2017**, *1*, 1232−1245.
(4) Furtado, A. C.; Alonso, C. G.; Cantão, M. P.; Fernandes-Machado, N. R. C. Bimetallic Catalysts Performance during Ethanol

Steam Reforming: Influence of Support Materials. *Int. J. Hydrogen Energy* **2009**, *34*, 7189−7196.

(5) Ni, M.; Leung, D. Y. C.; Leung, M. K. H. A Review on Reforming Bio-Ethanol for Hydrogen Production. *Int. J. Hydrogen Energy* **2007**, *32*, 3238−3247.

(6) Chen, J.; Sun, J.; Wang, Y. Catalysts for Steam Reforming of Bio-Oil: A Review. *Ind. Eng. Chem. Res.* **2017**, *56*, 4627−4637.

(7) Sharma, Y. C.; Kumar, A.; Prasad, R.; Upadhyay, S. N. Ethanol Steam Reforming for Hydrogen Production: Latest and Effective Catalyst Modification Strategies to Minimize Carbonaceous Deactivation. *Renewable Sustainable Energy Rev.* **2017**, *74*, 89−103.

(8) Alvarenga, G. M.; Villullas, H. M. Transition Metal Oxides in the Electrocatalytic Oxidation of Methanol and Ethanol on Noble Metal Nanoparticles. *Curr. Opin. Electrochem.* **2017**, *4*, 39−44.

(9) Kulesza, P. J.; Pieta, I. S.; Rutkowska, I. A.; Wadas, A.; Marks, D.; Klak, K.; Stobinski, L.; Cox, J. A. Electrocatalytic Oxidation of Small Organic Molecules in Acid Medium: Enhancement of Activity of Noble Metal Nanoparticles and Their Alloys by Supporting or Modifying Them with Metal Oxides. *Electrochim. Acta* **2013**, *110*, 474−483.

(10) Wang, Y.; Zou, S.; Cai, W.-B. Recent Advances on Electro-Oxidation of Ethanol on Pt- and Pd-Based Catalysts: From Reaction Mechanisms to Catalytic Materials. *Catalysts* **2015**, *5*, 1507−1534.

(11) Yue, H.; Ma, X.; Gong, J. An Alternative Synthetic Approach for Efficient Catalytic Conversion of Syngas to Ethanol. *Acc. Chem. Res.* **2014**, *47*, 1483−1492.

(12) Gupta, M.; Smith, M. L.; Spivey, J. J. Heterogeneous Catalytic Conversion of Dry Syngas to Ethanol and Higher Alcohols on Cu-Based Catalysts. *ACS Catal.* **2011**, *1*, 641−656.

(13) Spivey, J. J.; Egbebi, A. Heterogeneous Catalytic Synthesis of Ethanol from Biomass-Derived Syngas. *Chem. Soc. Rev.* **2007**, *36*, 1514.

(14) Hoydonckx, H. E.; De Vos, D. E.; Chavan, S. A.; Jacobs, P. A. Esterification and Transesterification of Renewable Chemicals. *Top. Catal.* **2004**, *27*, 83−96.

(15) Stergiou, P.-Y.; Foukis, A.; Filippou, M.; Koukouritaki, M.; Parapouli, M.; Theodorou, L. G.; Hatziloukas, E.; Afendra, A.; Pandey, A.; Papamichael, E. M. Advances in Lipase-Catalyzed Esterification Reactions. *Biotechnol. Adv.* **2013**, *31*, 1846−1859.

(16) Zhang, J.; Chen, W.; Feng, Y.; Wu, J.; Yu, J.; He, J.; Zhang, J. Homogeneous Esterification of Cellulose in Room Temperature Ionic Liquids. *Polym. Int.* **2015**, *64*, 963−970.

(17) Zhou, Y.; Niu, S.; Li, J. Activity of the Carbon-Based Heterogeneous Acid Catalyst Derived from Bamboo in Esterification of Oleic Acid with Ethanol. *Energy Convers. Manage.* **2016**, *114*, 188−196.

(18) Xu, B.; Madix, R. J.; Friend, C. J. Achieving Optimum Selectivity in Oxygen Assisted Alcohol Cross-Coupling on Gold. *J. Am. Chem. Soc.* **2010**, *132*, 16571−16580.

(19) Meng, Q. S.; Shen, Y. L.; Xu, J.; Gong, J. L. Mechanistic Insights into Selective Oxidation of Ethanol on Au(111): A DFT Study. *Chin. J. Catal.* **2012**, *33*, 407−415.

(20) Li, H.; Evans, E. J.; Mullins, C. B.; Henkelman, G. Ethanol Decomposition on Pd-Au Alloy Catalysts. *J. Phys. Chem. C* **2018**, *122*, 22024−22032.

(21) Li, H.; Henkelman, G. Dehydrogenation Selectivity of Ethanol on Close-Packed Transition Metal Surfaces: A Computational Study of Monometallic, Pd/Au, and Rh/Au Catalysts. *J. Phys. Chem. C* **2017**, *121*, 27504−27510.

(22) Evans, E. J.; Li, H.; Yu, W.-Y.; Mullen, G. M.; Henkelman, G.; Mullins, C. B. Mechanistic Insights on Ethanol Dehydrogenation on Pd−Au Model Catalysts: A Combined Experimental and DFT Study. *Phys. Chem. Chem. Phys.* **2017**, *19*, 30578−30589.

(23) Blöchl, P. E. Projector Augmented-Wave Method. *Phys. Rev. B: Condens. Matter Mater. Phys.* **1994**, *50*, 17953−17979.

(24) Perdew, J. P.; Burke, K.; Ernzerhof, M. Generalized Gradient Approximation Made Simple. *Phys. Rev. Lett.* **1996**, *77*, 3865−3868.

(25) Pople, J. A.; Gill, P. M. W.; Johnson, B. G. Kohn—Sham Density-Functional Theory within a Finite Basis Set. *Chem. Phys. Lett.* **1992**, *199*, 557−560.

(26) Henkelman, G.; Uberuaga, B. P.; Jónsson, H. A Climbing Image Nudged Elastic Band Method for Finding Saddle Points and Minimum Energy Paths. *J. Chem. Phys.* **2000**, *113*, 9901−9904.

(27) Li, H.; Shin, K.; Henkelman, G. Effects of Ensembles, Ligand, and Strain on Adsorbate Binding to Alloy Surfaces. *J. Chem. Phys.* **2018**, *149*, 174705.

(28) Li, H.; Luo, L.; Kunal, P.; Bonifacio, C. S.; Duan, Z.; Yang, J. C.; Humphrey, S. M.; Crooks, R. M.; Henkelman, G. Oxygen Reduction Reaction on Classically Immiscible Bimetallics: A Case Study of RhAu. *J. Phys. Chem. C* **2018**, *122*, 2712−2716.

(29) Guo, H.; Li, H.; Jarvis, K.; Wan, H.; Kunal, P.; Dunning, S. G.; Liu, Y.; Henkelman, G.; Humphrey, S. M. Microwave-Assisted Synthesis of Classically Immiscible Ag−Ir Alloy Nanoparticle Catalysts. *ACS Catal.* **2018**, *8*, 11386−11397.

(30) Yu, W.-Y.; Zhang, L.; Mullen, G. M.; Henkelman, G.; Mullins, C. B. Oxygen Activation and Reaction on Pd−Au Bimetallic Surfaces. *J. Phys. Chem. C* **2015**, *119*, 11754−11762.

(31) Liu, Y.; Li, H.; Cen, W.; Li, J.; Wang, Z.; Henkelman, G. A Computational Study of Supported Cu-Based Bimetallic Nanoclusters for CO Oxidation. *Phys. Chem. Chem. Phys.* **2018**, *20*, 7508−7513.

(32) Piburn, G. W.; Li, H.; Kunal, P.; Henkelman, G.; Humphrey, S. M. Rapid Synthesis of Rhodium−Palladium Alloy Nanocatalysts. *ChemCatChem* **2018**, *10*, 329−333.

(33) Kunal, P.; Li, H.; Dewing, B. L.; Zhang, L.; Jarvis, K.; Henkelman, G.; Humphrey, S. M. Microwave-Assisted Synthesis of Pd$_x$Au$_{100-x}$ Alloy Nanoparticles: A Combined Experimental and Theoretical Assessment of Synthetic and Compositional Effects upon Catalytic Reactivity. *ACS Catal.* **2016**, *6*, 4882−4893.

(34) Yu, W.-Y.; Zhang, L.; Mullen, G. M.; Evans, E. J.; Henkelman, G.; Mullins, C. B. Effect of Annealing in Oxygen on Alloy Structures of Pd−Au Bimetallic Model Catalysts. *Phys. Chem. Chem. Phys.* **2015**, *17*, 20588−20596.

(35) Kim, H. Y.; Henkelman, G. CO Adsorption-Driven Surface Segregation of Pd on Au/Pd Bimetallic Surfaces: Role of Defects and Effect on CO Oxidation. *ACS Catal.* **2013**, *3*, 2541−2546.

(36) Ferguson, B. A.; Reeves, C. T.; Mullins, C. B. Oxygen Adsorption on Si(100)-2 × 1 via Trapping-Mediated and Direct Mechanisms. *J. Chem. Phys.* **1999**, *110*, 11574.

(37) Wheeler, M. C.; Seets, D. C.; Mullins, C. B. Kinetics and Dynamics of the Initial Dissociative Chemisorption of Oxygen on Ru(001). *J. Chem. Phys.* **1996**, *105*, 1572.

(38) Koel, B. E.; Sellidj, A.; Paffett, M. T. Ultrathin Films of Pd on Au(111): Evidence for Surface Alloy Formation. *Phys. Rev. B: Condens. Matter Mater. Phys.* **1992**, *46*, 7846−7856.

(39) Xu, Z. F.; Wang, Y. Effects of Alloyed Metal on the Catalysis Activity of Pt for Ethanol Partial Oxidation: Adsorption and Dehydrogenation on Pt3M (M = Pt, Ru, Sn, Re, Rh, and Pd). *J. Phys. Chem. C* **2011**, *115*, 20565−20571.

(40) Zanchet, D.; Santos, J. B. O.; Damyanova, S.; Gallo, J. M. R.; Bueno, J. M. C. Toward Understanding Metal-Catalyzed Ethanol Reforming. *ACS Catal.* **2015**, *5*, 3841−3863.

(41) Zope, B. N.; Hibbitts, D. D.; Neurock, M.; Davis, R. J. Reactivity of the Gold/Water Interface During Selective Oxidation Catalysis. *Science (Washington, DC, U. S.)* **2010**, *330*, 74−78.

(42) Wang, H.-F.; Liu, Z.-P. Comprehensive Mechanism and Structure-Sensitivity of Ethanol Oxidation on Platinum: New Transition-State Searching Method for Resolving the Complex Reaction Network. *J. Am. Chem. Soc.* **2008**, *130*, 10996−11004.

(43) Liu, X.; Xu, B.; Haubrich, J.; Madix, R. J.; Friend, C. M. Surface-Mediated Self-Coupling of Ethanol on Gold. *J. Am. Chem. Soc.* **2009**, *131*, 5757−5759.

(44) Xu, B.; Liu, X.; Haubrich, J.; Friend, C. M. Vapour-Phase Gold-Surface-Mediated Coupling of Aldehydes with Methanol. *Nat. Chem.* **2010**, *2*, 61−65.

(45) Bürgstein, M. R.; Berberich, H.; Roesky, P. W. Homoleptic Lanthanide Amides as Homogeneous Catalysts for Alkyne Hydro-

amination and the Tishchenko Reaction. *Chem. - Eur. J.* **2001**, *7*, 3078−3085.

(46) Chen, B.; Wang, L.; Gao, S. Recent Advances in Aerobic Oxidation of Alcohols and Amines to Imines. *ACS Catal.* **2015**, *5*, 5851−5876.

(47) Xu, C.; Zhang, C.; Li, H.; Zhao, X.; Song, L.; Li, X. An Overview of Selective Oxidation of Alcohols: Catalysts, Oxidants and Reaction Mechanisms. *Catal. Surv. Asia* **2016**, *20*, 13−22.

(48) Besson, M.; Gallezot, P. Selective Oxidation of Alcohols and Aldehydes on Metal Catalysts. *Catal. Today* **2000**, *57*, 127−141.

(49) Opre, Z.; Grunwaldt, J.-D.; Mallat, T.; Baiker, A. Selective Oxidation of Alcohols with Oxygen on Ru−Co-Hydroxyapatite: A Mechanistic Study. *J. Mol. Catal. A: Chem.* **2005**, *242*, 224−232.

(50) Song, C.; Qu, S.; Tao, Y.; Dang, Y.; Wang, Z.-X. DFT Mechanistic Study of Ru II -Catalyzed Amide Synthesis from Alcohol and Nitrile Unveils a Different Mechanism for Borrowing Hydrogen. *ACS Catal.* **2014**, *4*, 2854−2865.

(51) Chmely, S. C.; Kim, S.; Ciesielski, P. N.; Jiménez-Osés, G.; Paton, R. S.; Beckham, G. T. Mechanistic Study of a Ru-Xantphos Catalyst for Tandem Alcohol Dehydrogenation and Reductive Aryl-Ether Cleavage. *ACS Catal.* **2013**, *3*, 963−974.

(52) Murcia, J. J.; Hidalgo, M. C.; Navío, J. A.; Vaiano, V.; Ciambelli, P.; Sannino, D. Photocatalytic Ethanol Oxidative Dehydrogenation over Pt/TiO₂Effect of the Addition of Blue Phosphors. *Int. J. Photoenergy* **2012**, *2012*, 1−9.

(53) Keresszegi, C.; Mallat, T.; Grunwaldt, J.-D.; Baiker, A. A Simple Discrimination of the Promoter Effect in Alcohol Oxidation and Dehydrogenation over Platinum and Palladium. *J. Catal.* **2004**, *225*, 138−146.

(54) Jin, X.; Taniguchi, K.; Yamaguchi, K.; Mizuno, N. Au−Pd Alloy Nanoparticles Supported on Layered Double Hydroxide for Heterogeneously Catalyzed Aerobic Oxidative Dehydrogenation of Cyclohexanols and Cyclohexanones to Phenols. *Chem. Sci.* **2016**, *7*, 5371−5383.

(55) Simakova, O. A.; Murzina, E. V.; Mäki-Arvela, P.; Leino, A.-R.; Campo, B. C.; Kordás, K.; Willför, S. M.; Salmi, T.; Murzin, D. Y. Oxidative Dehydrogenation of a Biomass Derived Lignan − Hydroxymatairesinol over Heterogeneous Gold Catalysts. *J. Catal.* **2011**, *282*, 54−64.

(56) Nowicka, E.; Hofmann, J. P.; Parker, S. F.; Sankar, M.; Lari, G. M.; Kondrat, S. A.; Knight, D. W.; Bethell, D.; Weckhuysen, B. M.; Hutchings, G. J. In Situ Spectroscopic Investigation of Oxidative Dehydrogenation and Disproportionation of Benzyl Alcohol. *Phys. Chem. Chem. Phys.* **2013**, *15*, 12147.

(57) Lee, A. F.; Naughton, J. N.; Liu, Z.; Wilson, K. High-Pressure XPS of Crotyl Alcohol Selective Oxidation over Metallic and Oxidized Pd(111). *ACS Catal.* **2012**, *2*, 2235−2241.

(58) Stoltz, B. M. Palladium Catalyzed Aerobic Dehydrogenation: From Alcohols to Indoles and Asymmetric Catalysis. *Chem. Lett.* **2004**, *33*, 362−367.

(59) Wang, M.; Wang, F.; Ma, J.; Li, M.; Zhang, Z.; Wang, Y.; Zhang, X.; Xu, J. Investigations on the Crystal Plane Effect of Ceria on Gold Catalysis in the Oxidative Dehydrogenation of Alcohols and Amines in the Liquid Phase. *Chem. Commun.* **2014**, *50*, 292−294.

(60) Mullen, G. M.; Zhang, L.; Evans, E. J.; Yan, T.; Henkelman, G.; Mullins, C. B. Oxygen and Hydroxyl Species Induce Multiple Reaction Pathways for the Partial Oxidation of Allyl Alcohol on Gold. *J. Am. Chem. Soc.* **2014**, *136*, 6489−6498.

(61) Mullen, G. M.; Evans, E. J.; Sabzevari, I.; Long, B. E.; Alhazmi, K.; Chandler, B. D.; Mullins, C. B. Water Influences the Activity and Selectivity of Ceria-Supported Gold Catalysts for Oxidative Dehydrogenation and Esterification of Ethanol. *ACS Catal.* **2017**, *7*, 1216−1226.

(62) Guan, Y.; Hensen, E. J. M. Ethanol Dehydrogenation by Gold Catalysts: The Effect of the Gold Particle Size and the Presence of Oxygen. *Appl. Catal., A* **2009**, *361*, 49−56.

(63) Inui, K.; Kurabayashi, T.; Sato, S. Direct Synthesis of Ethyl Acetate from Ethanol Carried Out under Pressure. *J. Catal.* **2002**, *212*, 207−215.

(64) Colley, S. W.; Tabatabaei, J.; Waugh, K. C.; Wood, M. A. The Detailed Kinetics and Mechanism of Ethyl Ethanoate Synthesis over a Cu/Cr2O3 Catalyst. *J. Catal.* **2005**, *236*, 21−33.

(65) Santacesaria, E.; Carotenuto, G.; Tesser, R.; Di Serio, M. Ethanol Dehydrogenation to Ethyl Acetate by Using Copper and Copper Chromite Catalysts. *Chem. Eng. J.* **2012**, *179*, 209−220.

(66) Zhang, M.; Li, G.; Jiang, H.; Zhang, J. Investigation on Process Mechanism on Cu−Cr Catalysts for Ethanol Dehydrogenation to Ethyl Acetate. *Catal. Lett.* **2011**, *141*, 1104−1110.

(67) Liu, J.; Lyu, H.; Chen, Y.; Li, G.; Jiang, H.; Zhang, M. Insights into the Mechanism of Ethanol Synthesis and Ethyl Acetate Inhibition from Acetic Acid Hydrogenation over Cu 2 In(100): A DFT Study. *Phys. Chem. Chem. Phys.* **2017**, *19*, 28083.

(68) Davis, J. L.; Barteau, M. A. The Influence of Oxygen on the Selectivity of Alcohol Conversion on the Pd(111) Surface. *Surf. Sci.* **1988**, *197*, 123−152.

(69) Davis, J. L.; Barteau, M. A. Decarbonylation and Decomposition Pathways of Alcohol's on Pd(111). *Surf. Sci.* **1987**, *187*, 387−406.

(70) Bowker, M.; Holroyd, R. P.; Sharpe, R. G.; Corneille, J. S.; Francis, S. M.; Goodman, D. W. Molecular Beam Studies of Ethanol Oxidation on Pd(110). *Surf. Sci.* **1997**, *370*, 113−124.

(71) Holroyd, R. P.; Bowker, M. Molecular Beam Studies of Alcohol (C₁-C₃) Adsorption and Reaction with Oxygen Pre-Covered Pd(110). *Surf. Sci.* **1997**, *377−379*, 786−790.

(72) Gong, J.; Mullins, C. B. Selective Oxidation of Ethanol to Acetaldehyde on Gold. *J. Am. Chem. Soc.* **2008**, *130*, 16458−16459.

(73) Han, S.; Mullins, C. B. Surface Alloy Composition Controlled O2 Activation on Pd−Au Bimetallic Model Catalysts. *ACS Catal.* **2018**, *8*, 3641−3649.

(74) Pan, M.; Flaherty, D. W.; Mullins, C. B. Low-Temperature Hydrogenation of Acetaldehyde to Ethanol on H-Precovered Au(111). *J. Phys. Chem. Lett.* **2011**, *2*, 1363−1367.

(75) Henderson, M. A.; Zhou, Y.; White, J. M. Polymerization and Decomposition of Acetaldehyde on Rutherium(001). *J. Am. Chem. Soc.* **1989**, *111*, 1185−1193.